Optimization and Comparison of Modern Offshore Wind Turbine Generators Using GeneratorSE 2.0

Preprint

Latha Sethuraman,[1] Garrett Barter,[1] Pietro Bortolotti,[1] Jonathan Keller,[1] and David A. Torrey[2]

1 National Renewable Energy Laboratory
2 General Electric Research

Presented at International Electric Machines and Drives Conference (IEMDC)
San Francisco, California
May 15–18, 2023

NREL is a national laboratory of the U.S. Department of Energy
Office of Energy Efficiency & Renewable Energy
Operated by the Alliance for Sustainable Energy, LLC

This report is available at no cost from the National Renewable Energy Laboratory (NREL) at www.nrel.gov/publications.

Contract No. DE-AC36-08GO28308

Conference Paper
NREL/CP-5000-85599
August 2023

Optimization and Comparison of Modern Offshore Wind Turbine Generators Using GeneratorSE 2.0

Preprint

Latha Sethuraman,[1] Garrett Barter,[1] Pietro Bortolotti,[1] Jonathan Keller,[1] and David A. Torrey[2]

1 National Renewable Energy Laboratory
2 General Electric Research

Suggested Citation
Sethuraman, Latha, Garrett Barter, Pietro Bortolotti, Jonathan Keller, and David A. Torrey. 2023. *Optimization and Comparison of Modern Offshore Wind Turbine Generators Using GeneratorSE 2.0: Preprint*. Golden, CO: National Renewable Energy Laboratory. NREL/CP-5000-85599. https://www.nrel.gov/docs/fy23osti/85599.pdf.

NREL is a national laboratory of the U.S. Department of Energy
Office of Energy Efficiency & Renewable Energy
Operated by the Alliance for Sustainable Energy, LLC

This report is available at no cost from the National Renewable Energy Laboratory (NREL) at www.nrel.gov/publications.

Contract No. DE-AC36-08GO28308

Conference Paper
NREL/CP-5000-85599
August 2023

National Renewable Energy Laboratory
15013 Denver West Parkway
Golden, CO 80401
303-275-3000 • www.nrel.gov

NOTICE

This work was authored in part by the National Renewable Energy Laboratory, operated by Alliance for Sustainable Energy, LLC, for the U.S. Department of Energy (DOE) under Contract No. DE-AC36-08GO28308. Funding provided by U.S. Department of Energy Office of Energy Efficiency and Renewable Energy Wind Energy Technologies Office. The views expressed herein do not necessarily represent the views of the DOE or the U.S. Government. The U.S. Government retains and the publisher, by accepting the article for publication, acknowledges that the U.S. Government retains a nonexclusive, paid-up, irrevocable, worldwide license to publish or reproduce the published form of this work, or allow others to do so, for U.S. Government purposes.

Cover Photos by Dennis Schroeder: (clockwise, left to right) NREL 51934, NREL 45897, NREL 42160, NREL 45891, NREL 48097, NREL 46526.

Optimization and comparison of modern offshore wind turbine generators using GeneratorSE 2.0

Latha Sethuraman
National Wind Technology Center
National Renewable Energy Laboratory
Golden, CO 80401
Latha.Sethuraman@nrel.gov

Garrett Barter
National Wind Technology Center
National Renewable Energy Laboratory
Golden, CO 80401
Garrett.Barter@nrel.gov

Pietro Bortolotti
National Wind Technology Center
National Renewable Energy Laboratory
Golden, CO 80401
Pietro.Bortolotti@nrel.gov

Jonathan Keller
National Wind Technology Center
National Renewable Energy Laboratory
Golden, CO 80401
Jonathan.Keller@nrel.gov

David A. Torrey
General Electric Research
One Research Circle
Niskayuna, NY 12309
torrey@ge.com

***Abstract*—As the offshore wind industry keeps growing at a rapid pace, developers are bracing themselves for a huge demand in critical rare earth metals which will threaten an already vulnerable supply chain. The wind energy industry is addressing this problem by investing in modern generator technologies that employ magnets with reduced rare earth content and high-field magnets enabled by rare-earth-free superconductors. In this paper we introduce the National Renewable Energy Laboratory's newly advanced GeneratorSE 2.0, which is a design and optimization tool that was developed to investigate the feasibility of such modern generators. Two direct-drive generator topologies with different magnet materials and mounting arrangements are investigated: an outer-rotor, V-shaped interior permanent magnet generator, and an inner-rotor normally conducting armature, paired with a low-temperature superconducting field with race-track coils. These technologies were evaluated for a range of power ratings between 15 and 25 MW, which represent the next generation of offshore wind turbines for both fixed-bottom and floating applications. The analyses indicate a new trend favoring the low-temperature superconducting technology for the direct-drive system.**

***Index Terms*—direct-drive generators, rare-earth-free magnets, superconductors**

I. Introduction

In recent years, the offshore wind industry has seen rapid growth in building powerful wind turbines—up to 15 MW—to achieve significant reductions in the levelized cost of electricity. As power ratings increase, key turbine components, including the generator, must also scale, creating new challenges in sourcing the raw materials, especially rare earth magnets [1]. To address this problem, wind turbine manufacturers are investing in advanced generator technologies, including the use of high-field reduced rare earth or rare-earth-free permanent magnet synchronous generators (PMSG) enabled by unique flux-enhancing topologies and superconductors [2]. Prior studies of these technologies have been restricted to conceptual designs or designs based on rare-earth-rich permanent magnets, or have precluded the economic feasibility of superconducting technology due to its high costs to commercialization [3], [4]. These comparative studies have also largely focused on high-temperature superconducting generators, ignoring low-temperature options. Further, they also focus on surface-mounted permanent magnet configuration for direct-drive systems, whose mass and costs grow significantly at higher power ratings and have increased risks of demagnetization, limiting their feasibility as a reduced rare earth permanent magnet solution. Barriers to overcoming these prior shortcomings are design approaches employing analytical methods that are limited in the ability to capture sensitivities related to different magnet grades or magnet mounting. Alternatively, higher-fidelity finite-element methods that effectively capture trade-offs in terms of mass, costs, and efficiency can be computationally intensive. Semi-analytical approaches offer a good compromise between computational efficiency and level of fidelity required to efficiently capture these sensitivities and is the approach adopted here.

In this study, we optimize and compare two types of large-scale reduced rare earth and rare-earth-free generators using GeneratorSE 2.0, a new implementation of NREL's semi-analytical framework for multiphysics optimization of generators [5]. The semi-analytical approach integrates simple analytical formulations for magnetic, structural, and basic thermal design with Finite Element Method Magnetics (FEMM) [6]. The open-source OpenMDAO library [7] serves as the glue code that assembles all the various components and provides the design optimization capability, as shown in Fig. 1. We choose to model select topologies of direct-drive superconducting generators and PMSGs and optimize them for fixed-bottom and floating wind turbines at five different power ratings—namely, 15, 17, 20, 22, and 25 MW.

The generators are designed for three-bladed upwind rotors with rated shaft torque and speed values calculated assuming

This research was funded by the U.S Department of Energy, Wind Energy Technologies Office

a rotor with specific power of 325 W/m^2 and rotor blade tip speed limit of 95 m/s. The generators were designed for a 3.3 kV (assuming at least two minimum turns per coil for PMSG and 1 turn per coil for superconducting generator), 60 Hz system for a certain target efficiency at rated operating torque. Table I lists the main design specifications for direct-drive interior PMSG (DD-IPMSG) and a direct-drive,low-temperature superconducting generator (DD-LTSG).

TABLE I
GENERATOR SPECIFICATIONS AND DESIGN BOUNDS

Parameter	***Symbol***	***Units***	**DD-IPMSG**	**DD-LTSG**
Magnet mounting	-	-	Outer rotor V-IPM	Outer stator racetrack
Rated voltage	V	kV	3.3	3.3
Target efficiency	η	%	95	97
Slot-pole	-	-	12-10	12-1
Number of phases	m	-	3	6
Magnet material	-	-	N48SH	NbTi
Physical air-gap	g	mm	7	60
Max. operation temperature	-	^{o}C	100	-269.15
Specific magnet cost	C_{PM}	\$/kg	66.75[a]	45.43[b]
Specific copper cost	C_{Fe}	\$/kg	7.30[c]	
Specific electrical steel cost	C_{Cu}	\$/kg	4.44[d]	
Specific structural steel cost	C_{st}	\$/kg	1.56[d]	
Magnet density	ρ_{PM}	kg/m^3	7600	NA
Copper density	ρ_{Cu}	kg/m^3	7300	
Electrical steel mass density	ρ_{Fe}	kg/m^3	7600	
Structural steel mass density	ρ_{Fes}	kg/m^3	7700	
Axial length	l_s	m	0.75–2.5	0.75–1.75
Stator radius	r_a/r_g	m	3.00–4.75	3.00–4.75
Pole pairs	pp	–	50–100	15–40
Magnet height	h_m/h_{sc}	mm	5–60	30–250
Initial field current	$I_{sc-input}$	A	-	650
Field coil turns	N_{sc}	-	-	1500–3500
Field coil width	d_α	deg	-	0.2–0.6
Stator/rotor yoke thickness	h_{ys}/h_{yr}	mm	20–300	150–300
Stator slot height	h_s	mm	50-400	50-400
Vertex-to-rotor inner radius	d_{mag}	mm	50–250	NA
Armature turns/coil	N_c	-	2–10	1–7
Tooth width	b_t	mm	20–100	20–100
Armature current density	$\hat{J}_s$	A/mm^2	≤ 6	

[a] metal.com/Rare-earth-Magnets/202103120034.
[b] Alibaba.com/showroom/superconducting-wire.html.
[c] moneymetals.com/copper-prices.
[d] agmetalminer.com/metal-p.

II. GENERATORSE 2.0 MODELS

Developed within the Wind-Plant Integrated System Design and Engineering Model (WISDEM), GeneratorSE 2.0 enables design optimization of direct-drive configurations of PMSG and LTSG (Low Temperature Superconducting Generator) at a wide range of power ratings. GeneratorSE receives turbine rotor torque, mechanical power, material properties, and specific costs as the key inputs, with constraints to satisfy targets for efficiency, terminal voltage, and magnetic field saturation. Each design is parameterized to create flexible 2-D cross-section geometry options that are evaluated for their electromagnetic characteristics in FEMM.

For the superconducting generator, we chose to model the low-temperature superconducting version with stationary field coils and normally conducting rotating armature consistent with the design described by Torrey [8].The LTSG option was chosen owing to its higher technology maturity, lower capital expense, commercially readiness, and established supply chain in comparison to HTS technology [9]. For the PMSG, we modeled an outer-rotor topology with magnets arranged in a V-shaped configuration owing to its superior performance against demagnetization, higher torque per unit volume, and increased magnetic loading than the surface-mounted PMSG [10]. For the structural design of the direct-drive generators, we used disc-type support structures consistent with the 15-MW reference generator [11]. The structures were constrained to deflect radially by no more than 20% of air-gap length.

We made a key modeling decision that no sizing of the cryogenic system or the torque tube and vacuum vessel was carried out. The mass and cost estimates on cooling requirements, for both technologies, were based on a previous study by General Electric [8] and scaled using regression approximations in WISDEM's Cost and Scaling Model. The absence of a thermal model is a known weakness of this study that should be addressed by a dedicated effort. All the conceptual designs used generator cost as the objective function through a common optimization strategy. To overcome the limitations in mesh-related solution convergence in FEMM, we used a gradient-free optimization solver with a combination of global search (using a differential evolution algorithm available through the OpenMDAO library) followed by local neighborhood search (using COBYLA algorithm).

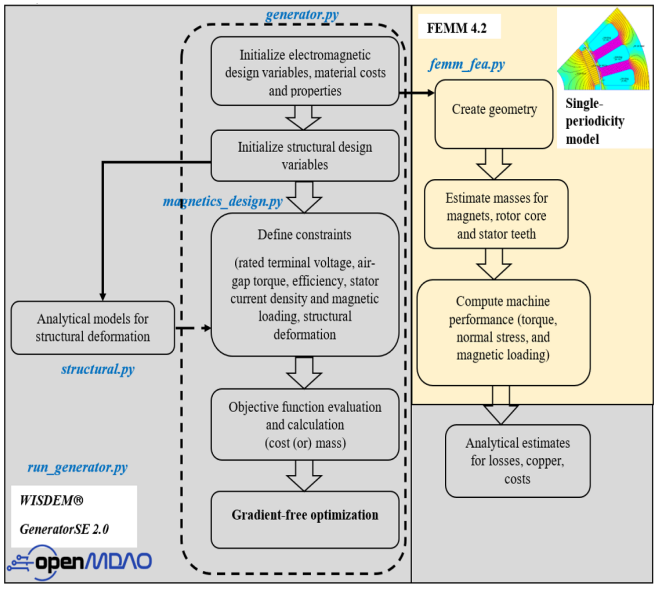

Fig. 1. GeneratorSE2.0 – A new semi-analytical framework for multiphysics optimization

A. DD-IPMSG sizing

The parameterization of the IPMSG is similar to the 15-MW reference generator layout that was updated for a single layer of magnets arranged in a V-shape (Fig. 1a). The stator design uses a three-phase, fractional slot layout and double-layer concentrated coils (with $q = 2/5$ slots per pole per phase) with peak value of stator current density input, $\hat{J}_s$, capped at 6 A/mm^2 to limit the thermal load on the machine design that is consistent with cooling using an air-to-air heat exchanger circuit [13]. The ratio of magnet pole arc-to-pole pitch was assumed to be 0.9. The magnet slots were simplified to a parallelogram with magnets filling the largest rectangular area possible within the available area. The choice of pole pairs influenced the magnet pole arc, magnet V-angle, magnet thickness, and the rotor yoke dimension. Each pair of magnets was oriented using the V-angle, α_v, which determines the lateral positions. The rotor magnets comprise N48SH-grade sintered, reduced dysprosium (smaller than 4% by weight) NdFeB magnets, with a remnant flux density of 1.4 T. With the maximum operation temperature limited to 100°C, the knee point for this magnet is slightly below 0.2 T. The stator and rotor yokes were assumed to be of M-36 grade steel with a saturation flux density of 2.15 T.

The design process followed the workflow as shown in Fig. 2 and was initialized by starting values for air-gap radius, stack length, number of pole pairs, yoke thicknesses, and stator slot dimensions for the chosen slot and pole geometry. The FEMM geometry was a single-periodicity model with 5 poles and 6 slots, and the machine segment was analyzed for both no-load conditions and full-load conditions. The sector angle for one machine segment was determined using $\theta = 5 \cdot 180/pp$. The total number of slots, S, is computed as $S = 6 \cdot pp \cdot (2/5)$ and used to determine the slot pitch as $\tau_s = \theta/6$.

The main electromagnetic design dimensions of the generator are obtained from an optimal choice of air-gap diameter and the axial length that are needed to produce the specific tangential force in N/m^2 generated by a given choice of pole pairs and stator phase currents. The stator is supplied with sinusoidal currents (by setting d-axis current, I_d, to zero, while q-axis current, I_q, is set to rated current). The electromagnetic torque, T_e, is computed using the Maxwell stress tensor from shear force per unit pole pitch, τ_p from stationary finite-element simulations that differ in relative positions between rotor and stator with armature current phase-shifted by the electrical frequency.

$$T_e = \frac{\pi D_g^2 l_s}{2\mu_o \tau_p} \int_0^{\tau_p} B_r B_t \, dl \tag{1}$$

where μ_0 is the permeability of free space, l_s is the axial length of stator laminations, D_g is the air-gap diameter, and B_r and B_t are the radial and tangential components of air-gap flux density, respectively. In FEMM, the torque is calculated by evaluating the integral in equation (1) and scaling the result by the sector angle for one periodicity. The stator design current was a derived parameter obtained from preset values of winding current density, useful slot area, and turns per coil as $I_n = 10^6 \hat{J}_s k_{fill} h_s b_s/(2N_c)$ with slot fill factor $K_{fill} = 65\%$ and slot width given by $b_s = 0.5\tau_s$. The first linear simulation is conducted by setting the stator currents to zero and leaving the permanent magnets magnetized. The resulting peak air-gap flux density, $\hat{B}_g$ is used to calculate the rms value of no-load line voltage:

$$E_p = \frac{1}{\sqrt{2}} \pi \hat{B}_g r_g l_s N_s k_{w1} \omega_m \tag{2}$$

This voltage is approximately 70%–110% of the rated phase voltage of the generator, with N_s being the stator turns per phase computed using $\frac{N_c S}{2m \cdot pp}$. The number of turns per coil, N_c, is optimized considering the fact that the sum of the back-electromotive forces and all voltage drops at rated speed and currents are equal to the rated terminal voltage using the phasor diagram as shown in Fig. 3. The fundamental winding factor, k_{w1}, for double-layer winding is computed to be 0.933 using Cro's technique [15]. The stator winding resistance per phase is calculated using the resistivity of copper at temperature 20°C as:

$$R_s = \frac{\rho_{Cu}(1 + (T_a - T_o)0.00393) L_{cus}}{A_{cus}} \tag{3}$$

The total coil length per phase including end-winding length is computed using $L_{cus} = (ls + \pi(\tau_s + b_t))/4$ and the conductor cross section, A_{cus}. Fig. 4 shows a closer look at the semi-closed, parallel-sided stator slot shape with slot opening width, tooth-tip dimensions, and slot leakage flux that were used to calculate the slot permeance function, λ_s, and stator magnetizing inductance [14]:

$$\lambda_s = \frac{h_s}{3b_s} + \frac{h_{so}}{0.5(b_s + b_{so})} + \frac{h_{so}}{3b_{so}} \tag{4}$$

The stator magnetizing inductance, L_{sm}, is approximated in equation (5) and will be added to slot leakage inductance, L_{sl}, and end-winding leakage, L_{ew}, using equations (6)–(7) [14]. The effective air gap, g_{eff}, was computed considering Carter's coefficient for stator slots.

$$L_{sm} = \frac{3\mu_0 (k_{w1} N_s)^2 D l_s}{pp^2 \pi g_{eff}} \tag{5}$$

$$L_{sl} = \frac{2\mu_0 (l_s N_s)^2}{pp^2 \pi g_{eff} l_s} \tag{6}$$

$$L_{ew} = \frac{\mu_0 (k_{w1} N_s)^2 2.4 l_{eav}}{S} \tag{7}$$

In computing the iron losses, P_{Fe}, the specific iron losses in different parts of teeth and yoke were passed to the Steinmetz formula (equation (8)), multiplied by the respective weights, and added.

$$P_{Fe} = M_{Fe}(2P_{Fe0h}\frac{f_e}{f_0}(\frac{B_{Fe}}{B_{Fo}})^2 + 2P_{Fe0e}(\frac{f_e}{f_0})^2(\frac{B_{Fe}}{B_{F0}})^2) \tag{8}$$

$$P_{PM} = P_{Ftm} \cdot 4pp \cdot l_s \cdot h_m \tag{9}$$

The frequency of the magnetic field in the iron mass f_0 = 60 Hz and specific hysteresis and eddy current losses were

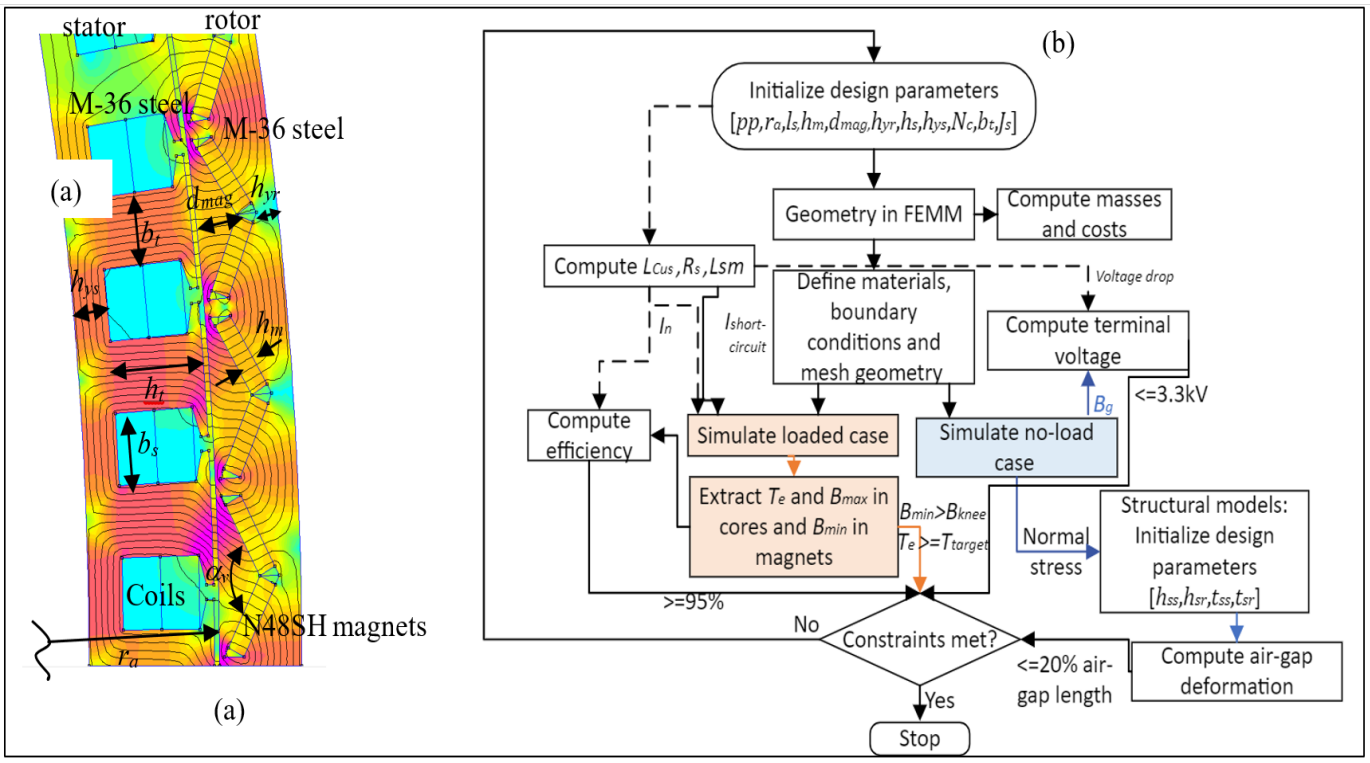

Fig. 2. (a) IPMSG design parameterization and (b) workflow

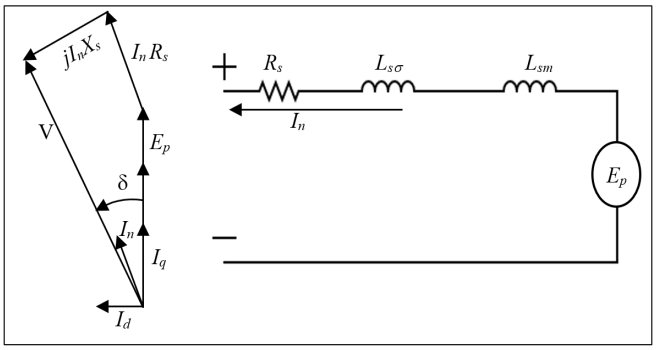

Fig. 3. Phasor diagram and steady-state equivalent circuit of IPMSG

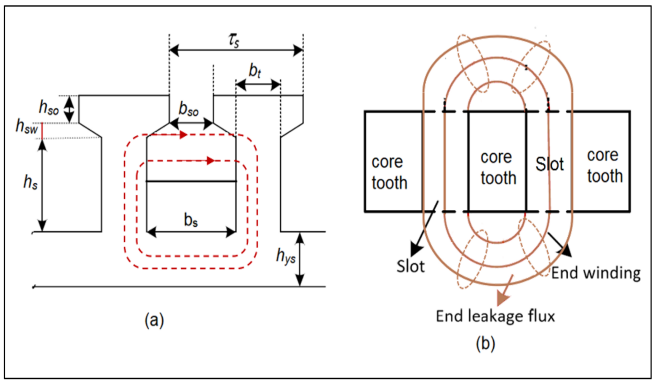

Fig. 4. Stator slot dimensions adapted from [14]

assumed at 4 kW/kg and 2 kW/kg.Considering the large dimensions of the magnets, losses from eddy currents in magnets were approximated in the form of specific magnet loss P_{Ftm} of 300 W/m^2 and multiplied by the pole dimensions. The losses were assumed to be small assuming radially laminated stacks that were also axially segmented. The overall generator efficiency is computed by accounting for additional iron losses from leakage flux (10% of total iron losses) as $\eta = 1-(1.1P_{Fe}+P_{Cu}+P_{pm})/P_{rated}$. The objective function was to minimize the sum total of costs of all materials.

The optimization was subject to constraints on target voltage, efficiency, torque, and maximum magnetic loading on stator and rotor cores given by :

$$\begin{aligned} \min \quad & Costs = C_{Cu}M_{Cu} + C_{Fe}(M_{Fes} + M_{Fer}) \\ & + C_{PM}M_{PM} + C_{st}M_{Fest} \\ \text{s.t.} \quad & \eta \geq \eta_{target} \\ & 0.9 \leq \frac{V}{V_{target}} \geq 1.1 \\ & 1.0 \leq \frac{T_e}{T_{target}} \\ & B_{max} \leq 2.53 \end{aligned} \tag{10}$$

The mass of stator copper, M_{Cu}, was obtained from the total winding length ($m\rho_{Cu}N_sL_{cus}A_{cus}$). The mass of stator and rotor electrical steel was determined from the stator and rotor areas (excluding magnet cavities) for one periodicity (A_s and A_r, respectively) and multiplied by the total number of peri-

odicities, N, as $M_{Fes} = \rho_{Fe} l_s A_s N$ and $M_{Fer} = \rho_{Fe} l_s A_r N$. The mass of magnets was similarly determined from magnet areas as $M_{PM} = \rho_{PM} l_s h_m l_m 4pp$. In determining the structural design and mass, the radial and axial deformations were analytically computed using formulations from [12] that were adapted for single-sided supports for both the stator and rotor structures. The normal components of Maxwell stress (σ_r) and shear stresses (σ_t) were computed from FEMM simulations by averaging the forces over one pole using equations (11) and (12) and applied to the stator and rotor rims as pressure loads:

$$\sigma_r = \frac{1}{2\mu_o \tau_p} \int_0^{\tau_p} ({B_r}^2 - {B_t}^2)\, dl \tag{11}$$

$$\sigma_t = \frac{2T_e}{\pi D_s^2 L_s} \tag{12}$$

B. DD-LTSG model

We selected an air-core, inner-rotor radial flux topology for the DD-LTSG architecture. This topology consists of an inner rotating armature assembly that holds conventional copper windings and an outer stationary field coil assembly of racetrack coils realized using neobium-titanium-copper (NbTi-Cu) composite conductors working at 4.2 K. The support frame of the armature is connected to the main shaft, and the power generated is fed via a full-rated converter through slip rings and brushes. The armature windings utilize a six-phase connection with two sets of three-phase windings displaced by 30º. A Roebelled bar winding layout was assumed to reduce the eddy current losses in the conductors. A magnetic yoke made of silicon steel behind the armature winding serves as a passive shield to improve the coupling between the field and armature. Because the rotor field strength is high enough to saturate commonly used iron cores, no magnetic materials were considered for the armature teeth or the rotor operating at cryogenic temperatures. The field coil conductor dimensions and critical current characteristics for the NbTi-Cu wires were provided by Bruker [18]. The design process followed the workflow as shown in Fig. 5 by initializing armature radius, stack length, pole pairs, yoke thicknesses, and field coil parameters. Only one pole was modeled with the boundary condition $dA_z/dn = 0$ applied to either sides of the pole, and the Dirichlet boundary condition was applied to the outer boundary.

The total number of periodicities is computed using ($N = pp$). The sector angle for one machine segment was determined using ($\theta_{lts} = 180/pp$). The armature winding has a double-layer distributed winding layout with 2 slots per pole per phase to create maximum magnetic symmetry. There are 12 slots per pole and a coil span of 10 slots to achieve a good balance of air-gap harmonics and winding factor. The total number of slots is computed as $S = 24\ pp$, and the slot pitch is computed as $\tau_s = \theta_{lts}/12$. In modeling the superconducting wires in FEMM, we assumed the superconductor inside a copper matrix with a Cu:SC ratio of 4.6. The surrounding medium was assumed to have a relative permeability of 1 and the superconductor has a relative permeability of zero. Then, the apparent bulk permeability was determined using the Ollendorff formula [17] that was simplified to $\mu_r = (1 - fill)/(1 + fill)$, where $fill$ is the volume fraction of the bulk winding that is occupied by the superconductor. The armature is forced-air-cooled to limit the working temperature below 160°C. The field coil assembly is cooled by liquid helium in a manner similar to magnetic resonance imaging technology where the racetrack is cooled using a single cylindrical cryostat.

The main electromagnetic design dimensions of the generator are obtained from an optimal choice of air-gap diameter and the axial length that are needed to overcome the specific tangential force in N/m^2 generated by the field coils and stator phase currents. In determining the field coil dimensions, the winding geometry ensured no overlap of the coils. The length of armature winding per turn is approximated using the geometry [19] as shown in Fig. 6.

$$l_{end} = \frac{4 l_{ew}}{sin\beta} \tag{13}$$

$$l_a w = 2l_s + 8l_{end} = 2l_s + 8(\frac{\tau_y}{2} tan\beta) \tag{14}$$

The armature phase resistance is then computed from the total length of armature coils per phase $L_{cus} = \frac{S}{mN_c l_a}$ and conductor cross section using equation (3). In computing the lengths for the field coil, the wire length for one racetrack is determined and multiplied by the number of turns, $l_{sc} = N_{sc}(2l_s + \pi(a_m + w_{sc}))$. The generator phase voltage was computed similar to the IPMSG model but scaled by a factor of 10% to account for contributions from the end windings. A winding factor $k_{w1} = 0.966$ was used for a coil span of 10 slots. The electromagnetic torque, T_e, is computed from a loaded simulation using equation (1). The end windings and overlap of coils between the segments also contributed to approximately 10% of air-gap torque, which was separately verified by 3-D modeling.

The working point of superconducting magnets was chosen to be within an operating margin chosen to vary within 80%–95% of critical current. The effective air-gap length was held constant at 60 mm to provide for sufficient allowance for these elements that were absent from the FEMM model. Generator efficiency was computed considering only winding losses and iron losses in the armature yoke. AC losses in the superconducting coils and losses from cryostat walls were neglected due to the large effective air gap and the rapid decay in harmonics [19]. Mechanical losses from bearing friction, windage losses, and ventilator losses were approximated to be less than 1% of rated power. In estimating conductor mass for the field and armature coils and losses, references were again made to [19].

C. OPTIMIZATION RESULTS

Fig. 7 compares results of optimized generator designs for both technologies for power ratings from 15 to 25 MW. The pole counts for the DD-IPMSG designs were consistently higher than 100, whereas the DD-LTSG design resulted in less than 80 poles per design and were also axially smaller.

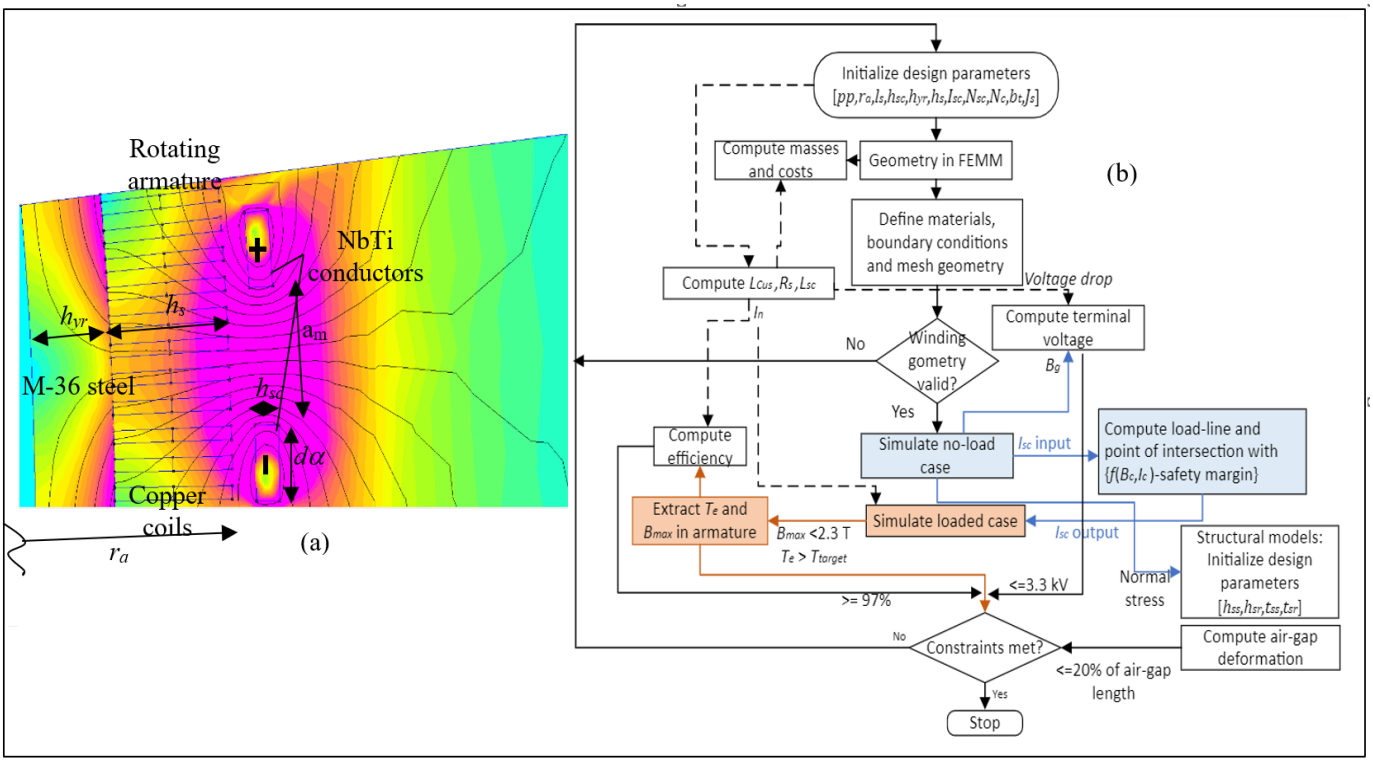

Fig. 5. (a) LTSG design parameterization and (b) workflow for LTSG

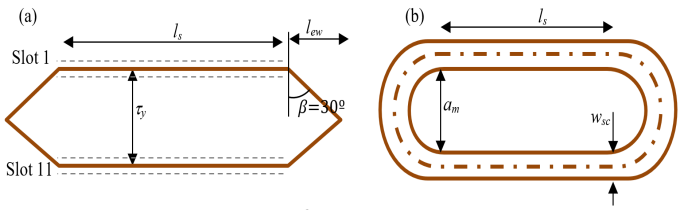

Fig. 6. Winding dimensions adaped from [19] (a) Armature (b) Field coil

Owing to the very large magnetic fields in air gap generated by the SC coils in the DD-LTSG system, despite the large effective mechanical air-gap and air-cored stator, the designs required only one-fifth the magnet mass when compared to DD-IPMSG. This also meant the use of up to 460 km of Nb-Ti tape per generator.

This demand is expected to be met, as the current annual production of these tapes is 300,000 km. For the DD-IPMSG, the magnet mass tended to scale quickly with an increase in power ratings, with more than 20 tons needed at power ratings exceeding 20 MW. This also necessitated a substantial increase in both active mass as well as structural mass at 25 MW to meet target specifications on torque. All DD-LTSG designs consistently met and exceeded the target efficiency constraints, whereas the DD-IPMSG designs were falling short. Results with a fill factor of 55% further reduced the efficiency by 1%. The authors anticipate improvements in efficiency with more optimized slot geometry and magnet dimensions. Despite the advantage of flux focusing to achieve high air-gap torques with DD-IPMSG, the generator mass climbs to as high as 500 tons at 25 MW. The fact that the DD-LTSG is substantially lighter helps attain almost double the torque-densities as compared to DD-IPMSG. If we assume that the two generator technologies are characterized by the same reliability, this study shows that DD-LTSG is a promising alternative to DD-PMSG for direct-drive offshore wind turbines. The significantly lower costs of LTSG are attributed to the difference in magnet costs. More competitive permanent-magnet-based generators at high torque densities using the direct-drive approach might entail nonconventional topologies such as Vernier machines or transverse-flux and axial-flux topologies. Enabling these alternatives might necessitate more reliable and demonstrated manufacturing with lower cost and high-performance reduced rare earth magnets.

ACKNOWLEDGMENT

This work was authored in part by the National Renewable Energy Laboratory, operated by Alliance for Sustainable Energy, LLC, for the U.S. Department of Energy (DOE) under Contract No. DE-AC36-08GO28308. Funding provided by the U.S. Department of Energy Office of Energy Efficiency and Renewable Energy Wind Energy Technologies Office. The views expressed in the article do not necessarily represent the views of the DOE or the U.S. Government. The U.S. Government retains and the publisher, by accepting the article for publication, acknowledges that the U.S. Government retains a nonexclusive, paid-up, irrevocable, worldwide license

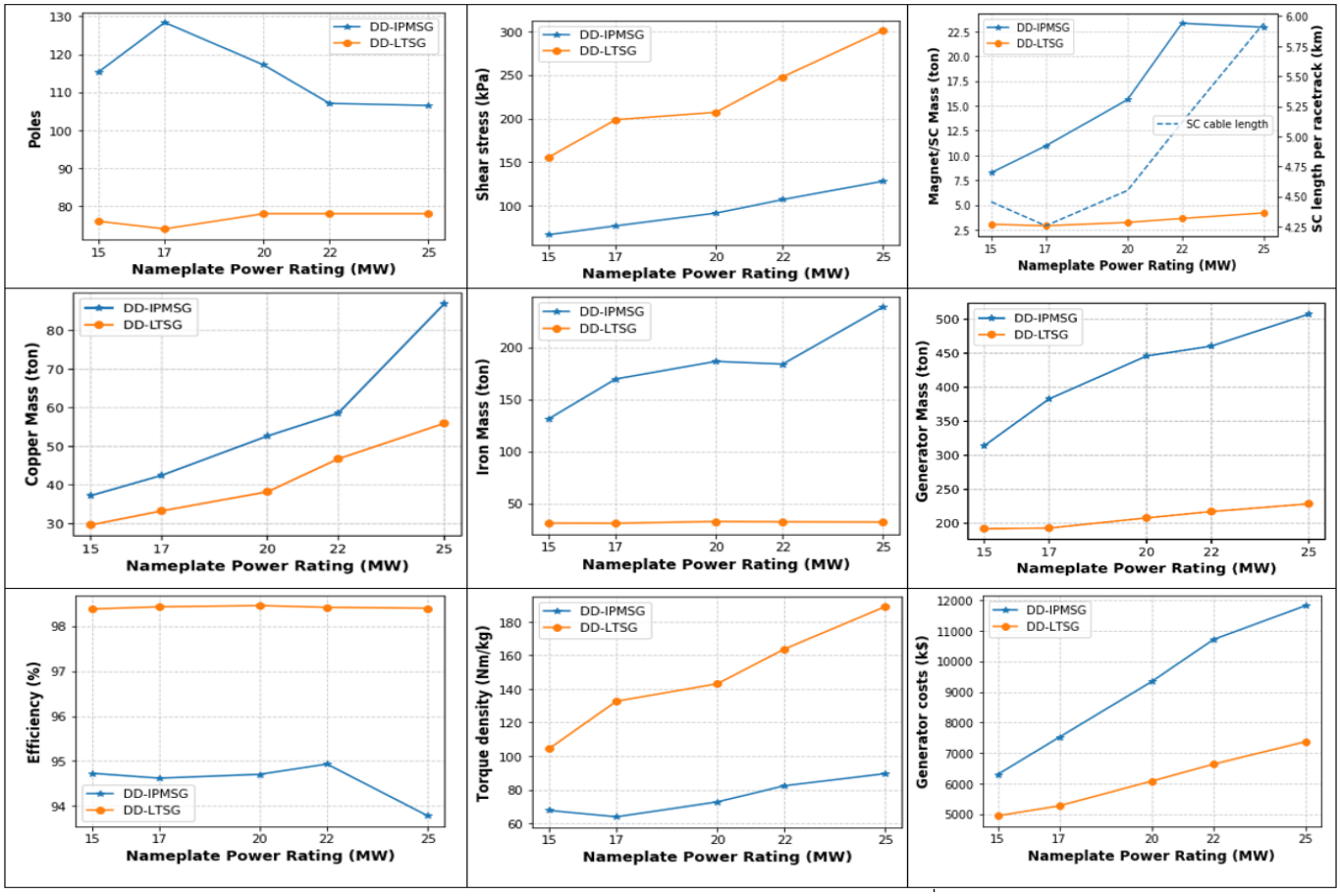

Fig. 7. Comparison of results from DD-IPMSG and DD-LTSG

to publish or reproduce the published form of this work, or allow others to do so, for U.S. Government purposes.

REFERENCES

[1] C. Li, J. M. Mogollón, A. Tukker, J. Dong, D. von Terzi, C. Zhang, B. Steubing, "Future material requirements for global sustainable offshore wind energy development," Renewable and Sustainable Energy Reviews, vol. 164, August 2022.

[2] J. Dodd, Rethinking the use of rare-earth elements.Wind Power Monthly, 2018. Available at https://www.windpowermonthly.com/article/1519221/rethinking-use-rare-earth-elements.

[3] T. Hoang, L. Queval, L. Vido, and D.Q. Nguyen. "Levelized cost of energy com-parison between permanent magnet and superconducting wind generators for various nominal power". IEEE Transactions on Applied Superconductivity, 32(7):1–6, 2022. doi: 10.1109/TASC.2022.3181996.

[4] S.K. Moore. Rough seas for the superconducting wind turbine: To keep offshore turbines light,engineers look beyond superconductors to a new permanent-magnet tech.IEEE Spectrum, 55(8):32–39,2018. doi: 10.1109/MSPEC.2018.8423581

[5] National Renewable Energy laboratory WISDEM GeneratorSE GitHub repository, 2022. Available at https://github.com/WISDEM/GeneratorSE.

[6] D. Meeker. Finite Element Method Magnetics (FEMM) 4.2, 2019.

[7] YJ. S. Gray, J. T. Hwang, J. R. R. A. Martins, K. T. Moore, and B. A. Naylor. OpenMDAO: An open-source framework for multidisciplinary design, analysis, and optimization. Structural and Multidisciplinary Optimization, 59(4):1075–1104, April 2019. doi: 10.1007/s00158 Available at https://www.femm.info

[8] D. Torrey, "Superconducting Generators for Offshore Wind Turbines." August 30, 2022, Available at https://www.nrel.gov/wind/assets/pdfs/.

[9] J. Wang, R. Qu, Y. Liu, J. He, Z. Zhu and H. Fang, "Comparison Study of Superconducting Wind Generators With HTS and LTS Field Windings," in IEEE Transactions on Applied Superconductivity, vol. 25, no. 3, pp. 1-6, June 2015, Art no. 5201806, doi: 10.1109/TASC.2014.2379697.

[10] H. Chen, R. Qu, J. Li and B. Zhao, "Comparison of interior and surface permanent magnet machines with fractional slot concentrated windings for direct-drive wind generators," 2014 17th International Conference on Electrical Machines and Systems (ICEMS), Hangzhou, China, 2014, pp. 2612-2617, doi: 10.1109/ICEMS.2014.7013942.

[11] E. Gaertner, J. Rinker, L. Sethuraman, F. Zahle, B. Anderson, G. Barter, et al, Definition of the IEA 15-megawatt offshore reference wind turbine. Technical Report NREL/TP-75698,International Energy Agency, 2020.

[12] A.McDonald, Structural analysis of low speed, high torque electrical generators for direct drive renewable energy converters, PhD Thesis, 2008.

[13] Heatex wind turbine cooling for 10+MW wind generator. Available at https://www.heatex.com/applications/wind-turbine-cooling/

[14] V. X.Hung, Modeling of exterior rotor permanent magnet machines with concentrated windings, PhD Thesis, TUDelft, 2012.

[15] J.Cro, P.Viarouge,Synthesis of high performance PM motors with concentrated windings, IEEE Transactions on energy conversion, Vol.17, No.2, 2002.

[16] V.X. Huang, Modeling of exterior rotor permanent magnet machines with concentrated windings, PhD Thesis, TUDelft,2012.

[17] F. Ollendorff. Magnetostatik der massekerne. Arch. Elektrotech. 1931, 25, 436–447.

[18] Bruker EST,NbTi conductors data sheet, 2021,made available via email inquiry.

[19] D.Liu, Design of a superconducting DC generator, PhD Thesis, KIT, 2018.